Inorg. Chem. **2005**, *44*, 3057–3062

Metal-Rich Chalcogenides. Synthesis, Structure, and Bonding of the Layered $Lu_{11}Te_4$. Comparison with the Similar Sc_8Te_3 and $Ti_{11}Se_4$

Ling Chen,[†,‡] Sheng-Qing Xia,[‡] and John D. Corbett*[,†]

Department of Chemistry, Iowa State University, Ames, Iowa 50011, and Fujian Institute of Research on the Structure of Matter, Chinese Academy of Sciences, Fuzhou, Fujian 350002, China

Received September 28, 2004

The high-yield synthesis of $Lu_{11}Te_4$ by reaction of the components and annealing at 1200 °C is described. The structure determined by single-crystal diffraction means is monoclinic *C*2/*m*, $Z = 6$, $a = 30.412(3)$ Å, $b = 3.9504(4)$ Å, $c = 21.073(2)$ Å, $\beta = 102.96°$ and consists of two independent condensed puckered sheets of Lu separated by individual Te atoms. Notwithstanding, the geometric structure is closely related to but distinctly different from those of both Sc_8Te_3 and $Ti_{11}Se_4$ (also *C*2/*m*), principally through displacements of pairs of atoms (the structure of the last was determined by electron diffraction). Further, close electronic similarities among the three structures are demonstrated by EHTB results in terms of both effective atom charge and bond overlap population trends between equivalent positions or functions.

Introduction

An unusual variety of metal-rich chalcogenides are found among the earliest transition metals. The earliest group III (rare-earth, R) metals Sc and Y as well as their heavier 4f analogues have been recent sources of a number of new metal-rich telluride structures. These generally feature novel chain or puckered sheet aggregates of metal that are more or less separated by a layer of individual chalcogenide atoms. The known structures can be divided into two groups: (1) those unique (so far) to Sc, Y, etc. and (2) those for which an electron-richer isotype is also stable for a group IV metal, Ti or Zr especially. The present paper reports on another possible example of the latter type for a $M_{11}Te_4$ stoichiometry.

The first example among the metal-rich rare-earth-metal chalcogenides, Sc_2Te[1] together with the later discovered Dy_2Te and Gd_2Te,[2] can be described in terms of 10-atom macrocluster sequences further condensed into infinite columns that are separated by telluride atoms. Örlygsson and Harbrecht subsequently showed that the analogous Zr_2Te also exists.[3] The microcrystalline phase β-Ti_2Se also has the same structure (although evidently not recognized as such) according to an electron diffraction structural analysis.[4]

The structure of the next metal-richer family contains two types of complex-puckered metal sheets separated by chalcogenide anions and occurs for Sc_8Te_3,[5] Y_8Te_3,[6] Ti_8S_3,[7] and Ti_8Se_3.[8] However, the latter two differ appreciably in detail because of the smaller anion spacers, a somewhat smaller metal core, and 44% more metal-based electrons, all of which serve to make the titanium analogues more strongly bound and also more 3D as the interactions across the chalcogenide gap become more important.[5] Of course, the same general differences also apply to Sc_2Te versus Zr_2Te. Two more low-dimensional phases are known among the known group III binary chalcogenide list. The new Y_7Te_2[9] has a previously unknown structure type, although it is the homometallic analogue of several isotypic orthorhombic Y_6MTe_2, M = Pd and Rh,[10] and analogous scandium phases Sc_6MTe_2, M = Pd, Ag, Cu, and Cd.[11,12] In addition, Sc_9Te_2 exhibits a rather distorted double-chain structure[13] that may conceivably

* Author to whom correspondence should be addressed. E-mail: jcorbett@iastate.edu.
† Iowa State University.
‡ Fujian Institute of Research on the Structure of Matter.

(1) Maggard, P. A.; Corbett, J. D. *Angew. Chem., Int. Ed. Engl.* **1997**, *36*, 1974.
(2) Herle, P. S.; Corbett, J. D. *Inorg. Chem.* **2001**, *40*, 1858.
(3) Örlygsson, G.; Harbrecht, B. *Inorg. Chem*. **1999**, *38*, 3377.
(4) Weirich, T. E.; Zhou, X.; Ramlau, R.; Simon, A.; Cascarano, G. L.; Giacovazzo, C.; Hovmöller, S. *Acta Crystallogr., Sect. A* **2000**, *56*, 29.
(5) Maggard, P. A.; Corbett, J. D. *Inorg. Chem.* **1998**, *37*, 814.
(6) Maggard, P. A.; Corbett, J. D. Unpublished research.
(7) Owens, J. P.; Franzen, H. F. *Acta Crystallogr., Sect. B* **1974**, *30*, 427.
(8) Weirich, T. E.; Pöttgen, R.; Simon, A. *Z. Kristallogr*. **1996**, *211*, 929.
(9) Castro-Castro, L. M.; Corbett, J. D. Unpublished research.
(10) Chen, L.; Castro-Castro, L. M.; Corbett, J. D. Unpublished research.
(11) Maggard, P. A.; Corbett, J. D. *J. Am. Chem. Soc.* **2000**, *122*, 10740.
(12) Chen, L.; Corbett, J. D. *Inorg. Chem.* **2002**, *41*, 2146.
(13) Maggard, P. A.; Corbett, J. D. *J. Am. Chem. Soc.* **2000**, *122*, 838.

10.1021/ic0401142 CCC: $30.25
Published on Web 03/25/2005

be related to that of higher symmetry Ti_9Se_2.[14] Finally, two unique 3D structures have been found for the even metal-richer lutetium−tellurium combinations Lu_8Te and Lu_7Te.[15] These are best described as hexagonal and orthorhombic derivatives of the hexagonal close-packed metal in which regular substitutions of tellurium for metal occur in rows normal to a simple close-packed direction.

We here report the newest addition to this collection, $Lu_{11}Te_4$, which to date has been found only with the heaviest lanthanide element. Its sheet structure further exhibits (a) a remarkably direct relationship to the Sc_8Te_3 structure (above) and (b) some comparable differences from that reported for $Ti_{11}Se_4$. The structure of the last was established through a careful electron diffraction study of the microcrystalline phase by Weirlich and co-workers.[16]

Experimental Procedures

Methods and techniques followed those described earlier.[5,13] Earlier synthetic explorations that ultimately led to the discoveries of Lu_7Te and Lu_8Te utilized a range of Lu/Te ratios. The arc-melted product of the 2:1 reaction contained 80% of what turned out to be $Lu_{11}Te_4$ plus LuTe (NaCl type). After the structure had been solved, a >95% pure sample of it was obtained (judging from the Guinier powder pattern) by the reaction of a stoichiometric mixture of Lu_2Te_3 and Lu. This utilized arc melting of a pressed pellet followed by annealing the result at 1300 °C for 48 h in a graphite-heated vacuum furnace with the sample wrapped in Mo foil and sealed within a Ta tube. The phase is shiny black and rather inert to air at room temperature. A similar procedure but with annealing at 1200 °C did not produce any $R_{11}Te_4$ phase for R = La, Pr, Sm, Gd, Ho, Tm, and Yb. The then-unknown phase $Lu_{11}Te_4$ was also seen earlier by S. Herle.[2]

Selected single crystals were examined on a Bruker APEX automatic diffractometer equipped with a CCD detector. The structure was solved and refined from data collected for the whole sphere of reciprocal space to $2\theta_{max} = 52.7°$ with 10 s/frame exposures. Space group *C*2/*m* was indicated, and the structure was readily solved therein by direct methods and refined with SHELXTL 6.10.[17] Absorption was corrected with the aid of the SADABS routine, giving 2760 independent reflections with $R_{int} = 0.072$. The final anisotropic refinement converged at $R1 = 0.0373$, $wR2 = 0.0717$ for $I_o > 2\sigma(I)$, with the highest ΔF residual peaks of 5.53 and −6.19 $e^-/Å^3$ located 0.71 and 0.81 Å from Lu7, respectively (see the following paragraph). There is no indication of a superstructure repeat along $\vec{b}$ at a $I/\sigma(I) > 5.0$ level. Results obtained from a second crystal were very similar. General crystal data, positional parameters, and nearest neighbor distances are given in Tables 1−3, respectively.

Only one small aspect of the refinement results bears note: Lu7 exhibits a somewhat larger value of the isotropic displacement ellipsoid U_{eq} (37×10^{-3} Å^2), which reflects mainly a large value of U_{33} (67×10^{-3}), and this is also evidenced by the largest residual peak (above). The effect of the U_{33} (and of the other *U* values) is to give an anisotropic displacement surface for Lu7 in the *a*−*c* plane that lies roughly normal to [001], with an aspect ratio of 2.9. An attempt to refine this perturbation as a disorder was not statistically significant; this reduced *R*1 by only 0.002 with a 75(6):24(6) proportion, resulted in positional standard deviations 5−20 times larger, and led to a component separation of only 0.62 Å. The feature is not attributable to an actual (and refineable) symmetry reduction to the acentric *C*2 space group either. Rather, it is observed that the U_{22} values for the closest neighbors Lu4 and Lu6 that lie in the direction of the Lu7 extension are unusually large too, with average aspect ratios of 4.0 and 4.9, respectively. This suggest a simple disorder model of six atoms, with pairs of bonded Lu7 atoms related by a 2-fold axis along *b* that are elongated along [001], plus pairs of Lu4 and Lu6 at their extremes quite elongated along [010] (see a later structural figure). With lighter atoms, this might be identified as a "asymmetric breathing mode", but here, it is better considered as just a soft correlated disorder. Interestingly, Sc_8Te_3 shows a very similar local atom arrangement around equivalent pairs of the original Sc15 (Sc7 as renumbered here) that are likewise elongated (aspect ratio of 2.4), but the secondary atom displacements of the Sc9 and Sc13 neighbors normal to that of Sc15 are only about half as extreme.[5]

Table 1. Some Crystal and Structure Refinement Data for $Lu_{11}Te_4$

f.u.	2435.07
crystal system, space group, *Z*	monoclinic, *C*2/*m* (no. 12), 6
unit-cell dimensions (Å, deg, Å^3)[a]	
a	30.412(3)
b	3.9504(4)
c	21.073(2)
β	102.960(2)
V	2467.2(4)
d_{calc} (Mg/m^3)	9.833
abs. coeff. (mm^{-1})	72.236
*R*1, *wR*2 [$I > 2\sigma(I)$]	0.0388, 0.0785
(all data)	0.0598, 0.0832
largest diff. peak and hole ($e^-/Å^3$)	5.53, −6.19

[a] CCD data.

Table 2. Atomic Coordinates ($\times 10^4$)[a] and Equivalent Isotropic Displacement Parameters ($Å^2 \times 10^3$) for $Lu_{11}Te_4$[b]

atom	*x*	*z*	*U*(eq)[c]	atom	*x*	*z*	*U*(eq)[c]
Lu(1)	4384(1)	4137(1)	10(1)	Lu(13)	321(1)	8345(1)	13(1)
Lu(2)	323(1)	4451(1)	11(1)	Lu(14)	4260(1)	383(1)	18(1)
Lu(3)	5359(1)	3075(1)	13(1)	Lu(15)	1273(1)	922(1)	12(1)
Lu(4)	1305(1)	3693(1)	15(1)	Lu(16)	5436(1)	1179(1)	12(1)
Lu(5)	6590(1)	2547(1)	13(1)	Lu(17)	0	0	22(1)
Lu(6)	2426(1)	3459(1)	19(1)	Te(1)	417(1)	6892(1)	9(1)
Lu(7)	2853(1)	5440(1)	37(1)	Te(2)	798(1)	2253(1)	12(1)
Lu(8)	1717(1)	5647(1)	13(1)	Te(3)	2161(1)	1943(1)	9(1)
Lu(9)	2547(1)	730(1)	9(1)	Te(4)	3417(1)	3282(1)	10(1)
Lu(10)	2041(1)	7811(1)	11(1)	Te(5)	3872(1)	5274(1)	14(1)
Lu(11)	8490(1)	957(1)	10(1)	Te(6)	6781(1)	199(1)	9(1)
Lu(12)	3939(1)	2213(1)	10(1)				

[a] $y = 0$. [b] All atoms lie in 4*i* (*m*) positions *x*, 0, *z*, except Lu17, which is on a 2/*m* site. [c] *U*(eq) is defined as one-third of the trace of the orthogonalized U_{ij} tensor.

Results and Discussion

The structure of $Lu_{11}Te_4$ shown in Figure 1 in a [010] projection has an overall characteristic already familiar for Sc_8Te_3 and its analogues, two types of puckered sheets of Lu (red and blue) interspersed with Te atoms (yellow). In fact, a close and direct interrelationship between $Lu_{11}Te_4$ and Sc_8Te_3 will be detailed shortly. All atoms in $Lu_{11}Te_4$ lie on mirror planes at $y = 0$ or $^1/_2$ and thus repeat every 3.95 Å. Somewhat more regularity is evident when it is noted that neighboring Lu atoms around the outside of the layered

(14) Weirich, T. E.; Pöttgen, R.; Simon, A. *Z. Anorg. Allg. Chem.* **1996**, *622*, 630.
(15) Chen, L.; Corbett, J. D. *J. Am. Chem. Soc.* **2003**, *125*, 7794.
(16) Weirich, T. E.; Ramlau, R.; Simon, A.; Hovmöller, S.; Zou X. *Nature* **1996**, *382*, 144.
(17) *SHELXTL 6.10*; Bruker AXS, Inc.: Madison, WI, 2000.

Table 3. Bond Lengths (Å) for $Lu_{11}Te_4$

Lu1−Te(4)		3.085(2)	Lu11−Lu14	×2	3.481(2)
Lu1−Te1	×2	3.098(2)	Lu11−L13	×2	3.585(2)
Lu1−Te5		3.137(2)	Lu12−Te4		3.031(2)
Lu1−Lu2	×2	3.412(2)	Lu12−Te1	×2	3.105(2)
Lu1−Lu2	×2	3.517(2)	Lu12−Lu11	×2	3.339(1)
Lu2−Te5	×2	3.098(2)	Lu12−Lu13	×2	3.397(2)
Lu2−Te1		3.195(2)	Lu12−Lu10	×2	3.566(2)
Lu2−Lu2		3.355(3)	Lu13−Te1		3.141(2)
Lu2−Lu1	×2	3.412(2)	Lu13−Lu14	×2	3.343(2)
Lu2−Lu1		3.517(1)	Lu13−Te2		3.352(3)
Lu2−Lu3	×2	3.530(2)	Lu13−Lu16	×2	23.354(2)
Lu2−Lu4		3.690(2)	Lu13−Lu12	×2	3.397(2)
Lu3−Te1	×2	3.092(2)	Lu13−Lu11		3.535(2)
Lu3−Te2	×2	3.117(2)	Lu13−Lu3	×2	3.789(2)
Lu3−Lu4	×2	3.493(2)	Lu13−Lu17		3.827(2)
Lu3−Lu2	×2	3.530(2)	Lu14−Te6		3.129(2)
Lu3−Lu13	×2	3.789(2)	Lu14−Lu17	×2	3.229(1)
Lu4−Te5	×2	3.075(2)	Lu14−Lu13	×2	3.343(2)
Lu4−Te2		3.081(2)	Lu14−Lu15	×2	3.478(2)
Lu4−Lu5	×2	3.379(2)	Lu14−Lu11	×2	3.481(2)
Lu4−Lu7	×2	3.419(2)	Lu14−Lu16		3.593(2)
Lu4−Lu3	×2	3.493(2)	Lu14−Lu16		3.612(2)
Lu4−Lu6		3.551(2)	Lu15−Te3		3.052(2)
Lu5−Te2	×2	3.070(2)	Lu15−Te6	×2	3.110(2)
Lu5−Te3	×2	3.086(2)	Lu15−Lu16	×2	3.359(2)
Lu5−Lu4	×2	3.379(2)	Lu15−Te2		3.430(2)
Lu5−Lu6	×2	3.444(2)	Lu15−Lu14		3.478(2)
Lu5−Lu15	×2	3.883(2)	Lu15−Lu5	×2	3.8823(2)
Lu6−Te3		3.114(2)	Lu15−Lu17		3.922(1)
Lu6−Te4		3.120(3)	Lu16−Te2	×2	3.020(2)
Lu6−Lu7	×2	3.299(2)	Lu16−Te2		3.021(2)
Lu6−Lu5		3.444(2)	Lu16−Lu17	×2	3.2186(1)
Lu6−Lu8	×2	3.470(2)	Lu16−Lu13	×2	3.354(2)
Lu7−Lu7	×2	3.188(3)	Lu16−Lu15	×2	3.359(2)
Lu7−Te5		3.197(3)	Lu16−Lu14		3.612(2)
Lu7−Lu6	×2	3.299(2)	Lu17−Lu16	×2	3.218(1)
Lu7−Lu4	×2	3.419(2)	Lu17−Lu14	×2	3.229(1)
Lu7−Lu8	×2	3.494(2)	Lu17−Lu13	×2	3.827(1)
Lu7−Lu8		3.577(2)	Lu17−Lu15		3.922(1)
Lu8−Te5	×2	3.053(2)	Te1−Lu1	×2	3.090(2)
Lu8−Te4	×2	3.095(2)	Te1−Lu3		3.092(2)
Lu8−Lu6	×2	3.470(2)	Te1−Lu12		3.105(2)
Lu8−Lu7	×2	3.494(2)	Te1−Lu2		3.195(2)
Lu9−Te3		3.043(2)	Te2−Lu16	×2	3.020(2)
Lu9−Te6	×2	3.068(2)	Te2−Lu5	×2	3.070(2)
Lu9−Te6		3.131(2)	Te2−Lu3	×2	3.117(2)
Lu9−Lu11	× 2	3.427(2)	Te2−Lu13		3.352(3)
Lu9−Lu9	× 2	3.613(2)	Te3−Lu10		3.081(2)
Lu9−Lu10	×2	3.633(2)	Te3−Lu5	×2	3.086(2)
Lu10−Te3	×2	3.081(2)	Te4−Lu8	×2	3.095(2)
Lu10−Te4	×2	3.116(2)	Te4−Lu10	×2	3.116(2)
Lu10−Lu11		3.3530(2)	Te5−Lu8	×2	3.053(2)
Lu10−Lu12		3.566(2)	Te5−Lu4	×2	3.075(2)
Lu10−Lu9	×2	3.633(2)	Te5−Lu2	×2	3.098(2)
Lu11−Te6	×2	3.099(2)	Te6−Lu9		3.068(2)
Lu11−Lu12		3.339(1)	Te6−Lu11	×2	3.099(2)
Lu11−Lu10		3.353(2)	Te6−Lu15	×2	3.110(2)
Lu11−Lu9		3.427(2)	Te6−Lu14		3.129(2)
			Te6−Lu9		3.131(2)

aggregates alternate between the mirror planes (this is especially clear in the red sheets). The lighter bonds seen in the interior of each chain mark neighbors that lie at the same heights in $\vec{b}$, and from this comes the most cogent organizing feature: the sheet structures can be generated from, first, infinite chains of octahedra that share trans edges (these central bonds) and run along $\vec{b}$ and, second, such chains that share some side (solid red or blue) edges to complete the aggregation. Finally, two isolated chains of single atoms, Lu3 and Lu9, bridge between such blocks in the respective chains. The blue chain is somewhat larger and more condensed, with one striking feature being four such chains of octahedra that

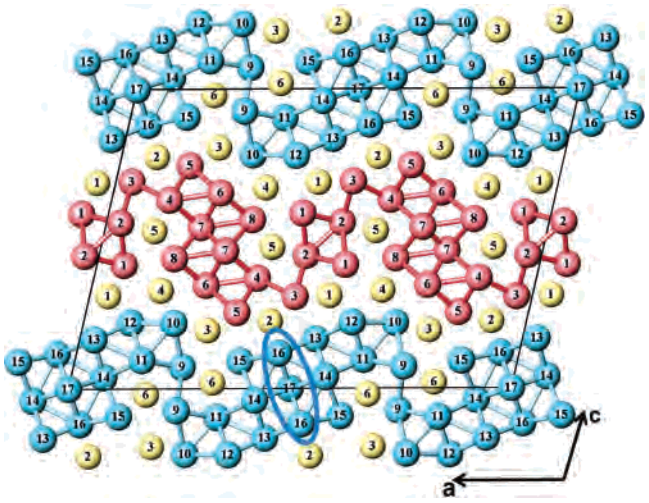

Figure 1. [010] projection of the structure of $Lu_{11}Te_4$ ($C2/m$) along the short (3.95 Å) b axis showing cross sections of the separate (red and blue) puckered lutetium layers. The intervening yellow atoms are tellurium. Lu−Lu contacts less than 3.62 Å are marked. Atoms in the circled Lu16−Lu17−Lu16 segment are displaced or removed on formation of the Sc_8Te_3-type structure (see the text and Figure 2).

share edges and a single vertex (Lu17) to generate chains of face-centered cubes. Similar square blocks are found directly connected in Sc_9Te_2.[13]

All Lu−Lu distances within 3.61 Å are marked in the drawing. As before,[5,13] more central Lu−Lu contacts within metal aggregates tend to be shorter [d(Lu7−Lu7) = 3.19 Å; d(Lu16−Lu17) = 3.22 Å], whereas those around atoms that have more bonding contacts with Te logically tend to be longer [d(Lu2 − Lu3) = 3.53 Å; d(Lu10 − Lu12) = 3.57 Å] (overlap populations are of course better measures of these covalency effects). The imagined shared waist edges within the octahedral chains are usually also longer but not always, depending on the packing and location.

This phase is more complex than its predecessors, to the extent that its very stability is a little surprising. Subtle differences among many factors must be involved. In addition to obvious Lu−Lu bond energies, the Madelung energies must be important. All of the tellurium atoms have fairly normal (common) 6−8 metal neighbors in the shape of augmented trigonal prisms.

Structural Comparisons. A surprisingly direct relationship between the $Lu_{11}Te_4$ structure and that of Sc_8Te_3 can be found, whereas its comparison with that of $Ti_{11}Se_4$ is also significant regarding both the similarities and contrasts. For these purposes, some crystal data for the three phases, all in space group $C2/m$, are compared in Table 4.

The similarity of the constitution of $Lu_{11}Te_4$ and Sc_8Te_3[6] can easily be seen on comparison of Figures 1 and 2. For the latter, the origin has been shifted by $c/2$ to an alternate choice, the orientation has been changed, and the atoms have been renumbered so as to follow the $Lu_{11}Te_4$ scheme as far as possible. The two structures differ numerically in the atom multiplicities and Z (Table 4). Specifically, a chain of three adjoining 4-fold Lu16 and 2-fold Lu17 (at the origin) are removed on going from $Lu_{11}Te_4$ to Sc_8Te_3, and a pair of 4-fold Sc16 are added around each equivalent Sc9−Sc9

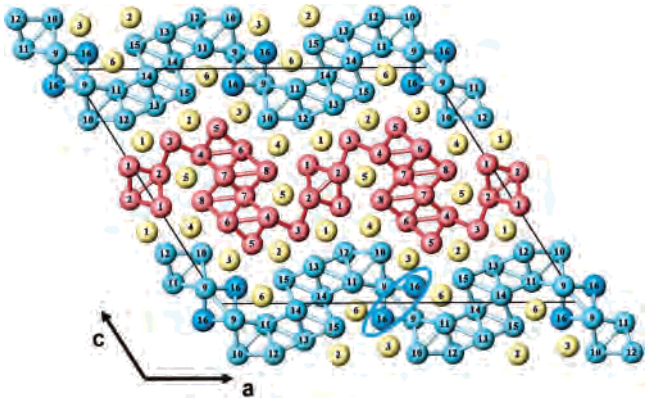

Figure 2. Comparative [010] view of the structure of Sc_8Te_3.[5] The origin has been displaced by $c/2$, the cell has been reoriented, and the atoms have been renumbered to correspond as closely as possible to the arrangement in $Lu_{11}Te_4$. Note the very similar arrangements of the red chains in the two. The blue chains here are generated from those in $Lu_{11}Te_4$ by removal of the Lu16−Lu17−Lu16 segment marked in Figure 1 and placement of the two Sc16 atoms around the Sc9−Sc9 bond. Both of these are circled in blue.

Table 4. Relationships between M_8Ch_3 and $M_{11}Ch_4$ Structures

	M_8Ch_3	$M_{11}Ch_4$	
space group	*C*2/*m*	*C*2/*m*	
Pearson symbol (*Z*)	*m*C88, 8	*m*C90, 6	
examples	Ti_8S_3, Ti_8Se_3 Sc_8Te_3,Y_8Te_3	$Lu_{11}Te_4$	$Ti_{11}Se_4$
references	7, 8, 5, 5	this paper	14
unit-cell dimensions (Å, deg)	Sc_8Te_3	$Lu_{11}Te_4$	$Ti_{11}Se_4$
a	28.842(7)	30.412(3)	25.52(1)
b	3.8517(6)	3.9504(4)	3.448(1)
c	22.352(5)	21.073(2)	19.201(6)
β	122.51(2)	102.960(2)	117.84(3)
structural method	single crystal X-ray	single crystal X-ray	electron microscopy
*R*1 (%)	3.7	3.9	14.7

bond. One of the former group is circled at the bottom of Figure 1, and one example of the latter is circled in Figure 2. The fact that these simple alterations relate these two structures is rather surprising considering the additional differences in metal sizes and bonding (see the comparisons of Sc_2Te and Dy_2Te[2]). The view in Figure 2 was chosen because it best presents the close similarities in conformations within the metal sheets, but the necessary change in the angle is striking. An appreciable difference follows in the interface between the two chain types, along which some slippage is evident. This can be seen, for example, in the interchain R5−R15 orientation as the Lu16, 17, and 16 group is removed.

A somewhat more complicated relationship exists between $Lu_{11}Te_4$ and $Ti_{11}Te_4$ despite the identical stoichiometries, yet their similarities are also very clear. The presence of smaller component atoms and a larger number of bonding electrons in $Ti_{11}Se_4$ are of course relevant, but the structural methods utilized in its study were also fundamentally different. The pioneering result for this titanium selenide structure came from a complete analysis by electron diffraction,[16] namely, high-resolution microscopy data that led to the model and selected area electron diffraction intensities that received standard least-square refinements ($R1 = 14.7\%$), all from a crystal of tens of nanometers in size and with the assumption

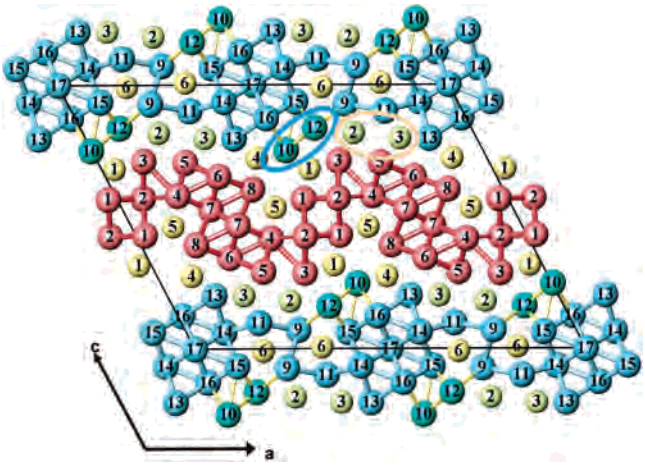

Figure 3. Comparable [010] view of the $Ti_{11}Se_4$ structure determined by electron microscopy with atoms renumbered to correspond to the arrangement or function in $Lu_{11}Te_4$, in Figure 1. The two structures are closely related by interchange of the M10−M12 and Ch2−Ch3 atom pairs (circled) (Ch = Te and Se).

of kinetic scattering (other structures have been solved since, through applications of direct methods alone to selected area data[4]).

The $Ti_{11}Se_4$ result[16] in Figure 3 compares with that for $Lu_{11}Te_4$, Figure 1, with the atoms in the former similarly renumbered. Bonds are drawn around the outside of the sheet structures for all Ti−Ti separations less than 3.10 Å (some interchain contacts of 3.16 Å are not marked). This view was again chosen to give the best comparisons of structures within the sheets. On the other hand, the substantial contrast in β angles when similar chain conformations are compared is again noteworthy, and slippage between metal sheets is clear. The red chains are again substantially identical to those in $Lu_{11}Te_4$ except for some additional bonds within the sheet for the smaller and electron-richer Ti, e.g., for Ti2−Ti4 (similar changes have also been seen for Sc_8Te_3 versus Ti_8Ch_3, Ch = S, Se[5]). Even so, the relationship of $Ti_{11}Se_4$ to $Lu_{11}Te_4$ is closer than it is to Sc_8Te_3 with a comparable β angle because of the difference in the composition of the last.

Changes in the blue chain are pictorially simple but still substantial; the Te2 and Te3 (Se2 and Se3) atoms (greenish yellow) and the M10 and M12 pair (blue green) at the intersheet boundary basically switch places between $Lu_{11}Te_4$ and $Ti_{11}Se_4$, as circled in orange and blue, respectively, in Figure 3. The first thins the metal sheet alongside M9 to M11, while the second thickens the layer on both sides of the 3 × 3 metal block composed of M13−M17. These changes also correlate with the relative position of M3 and M5 in the central chain, which more-or-less "follow" the chalcogen migration. The conformational changes in the more condensed blue sheet also serve to trap Se6 in a columnar cavity, an unusual event in this kind of compound but one with a quite regular structure.

It does not seem at all likely that the apparent migration of these atom pairs could originate with errors in the assignments in the electronic crystallography study, in as much as the new environments for these atoms in $Ti_{11}Se_4$

are clearly more suitable. Otherwise, the Se1, 2, and 4 region would contain unreasonably crowded anions in $Ti_{11}Se_4$, and the unmigrated Ti10 and 12 would be too close to Ti3 and 5 across the gap (−2.6 Å) and without intervening anions. In fact, all of the anions in the reported titanium structure have quite reasonable numbers of metal neighbors (7−9) and distances (2.5−2.7 Å). The reported structure has also been shown to lie close to a minimum in the total energy according to a refinement of the atom positions by DFT-GGA theoretical methods,[18] with the atomic coordinate shifts averaging only 0.04. They did not consider other possible energy minima, of course.

Calculations and Comparisons. The preceding qualitative visual comparisons between structural motifs and judgments about their interrelationships are common practice in chemical crystallography. We also sought further evidence that these structures did indeed exhibit common or parallel bonding characteristics and apparent charge distributions, particularly because of the variety of elements involved. The scandium and titanium chalcogenides entail relatively small cations and different electron counts, whereas the lutetium member incorporates a distinctly larger and more electropositive metal. The last engenders more significant Lu−Lu bonding interactions across the gap between sheets with a fixed anion, whereas some related effects in $Ti_{11}Se_4$ will arise with the smaller spacer and greater band filling.

Effective charges for all of the atoms in the three structures have been calculated by EHTB means[19] within the Mulliken approximation, viz., with the bonding electrons between all atom pairs divided equally (parameters utilized are listed in the Supporting Information). The approach is relatively simple, and too quantitative meanings should not be read into the results; nonetheless, the data are quite useful in a comparative sense between different atom types or sites or between different structures.

The relative charges are compared in Figure 4 for (b) Sc_8Te_3, (a) $Lu_{11}Te_4$, and (c) $Ti_{11}Se_4$, each as a function of the ID numbers of the atoms. The results for Sc_8Te_3 versus $Lu_{11}Te_4$ are quite parallel in the first pair, in as much as the environments are quite similar. The greater R−Ch covalency or lower polarity in Sc_8Te_3 is evident in a greater charge dispersion, more positive for those atoms with two Te neighbors (Sc3, 8, 10, and 15) and more negative for those buried in the metal net (Sc7, 9, 11, and 14). Similar effects have been inferred before, generally in terms of overlap populations[5,13] but less often in a comparative sense.[2,3] One major change is that the switched Sc16 has twice as many Te neighbors (4) and only Lu17 exists. The striking difference for atom 9 results from the fact that two Sc16 atoms now bracket the Sc9−Sc9 bond, reducing the number of tellurium near neighbors about R9 from four to one here. The fairly charge-invariant atoms 18−23 in both phases are tellurium, with slightly different functions in detail (Figures 1 and 2). A distinct alternation of apparent charge (or overlap

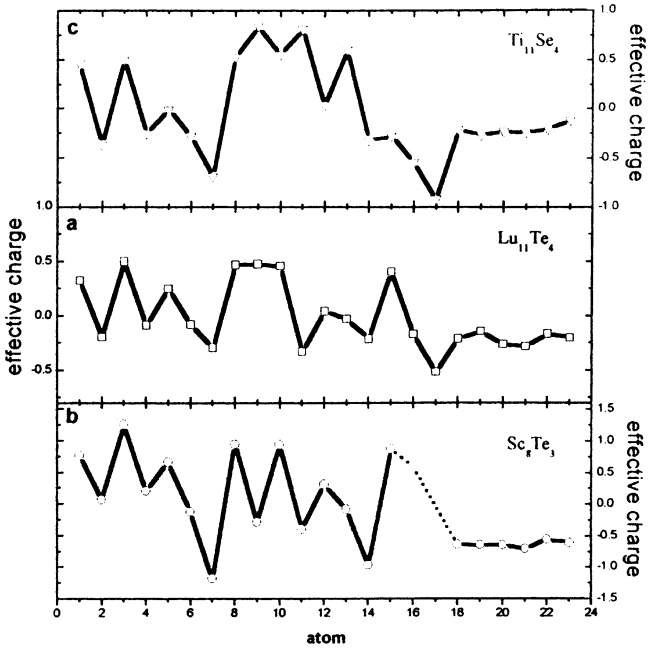

Figure 4. Comparison of effective atom charges (EHTB, Mulliken approximation) in (a) $Lu_{11}Te_4$, (b) Sc_8Te_3, and (c) $Ti_{11}Se_4$ by atom number as defined in the figures (The ordering of these parts is b, a, and c). Note both the similar trends with atom function and plausible differences (see the text). Major variations are discussed in the text.

population) is also noticeable in many of these line graphs. This simply arises from the zigzag periphery on the sheets, with alternate atoms projecting farther into the chalcogenide regions. All is fairly sensible.

The comparison of $Lu_{11}Te_4$ with $Ti_{11}Se_4$ would seem to be beset with complications because of the rearrangements already noted, in Figure 3. However, if the atoms are plotted as numbered in Figures 1 and 3, wherein the *atom function* is guiding and not the position, then the regularities are again evident, in parts a and c of Figure 4. The greater charge dispersion evidenced in $Ti_{11}Se_4$ is as before. As the structural pictures qualitatively indicate and the effective atom charges support, Ti15 and Ti16 become more bonded to Ti (and less to Se, particularly for Ti15) and thence the more negative and Ti9 does not change much, whereas the opposite effects are seen for Ti11 and Ti13 in the reorganization, with these becoming more bonded to Se and more positive (polar).

Overlap populations for R−R bonds afford even more similar trends as anion neighbors appear less influential. For $Lu_{11}Te_4$ versus Sc_8Te_3, in Figure 5a, the bonds are selected in parallel and placed in numeric order for R(a)−R(b) in which b > a (the order is listed in the Supporting Information). The only divergence that is noteworthy is for bonds 13 and 14, which correspond to R9−R9 and R9−R10, respectively. However, these effects can be easily understood in terms of the additional Sc16 atoms about Sc9 in the latter, in Figure 2.

The overlap population distribution for metal−metal bonds in $Lu_{11}Te_4$ versus $Ti_{11}Se_4$, in Figure 5b, follows very similar patterns because we compare the bonding of Lu11 and 12 against that for the transferred Ti10 and 12 (note that, here, we compare these by atom functions and not by number; see the table in the Supporting Information). A difference

(18) Weirich, T. E. *Acta Crystallogr., Sect. A* **2004**, *60*, 75.
(19) Ren, J.; Liang, W.; Whangbo, M.-H. *CAESAR for Windows*; Prime-Color Software, Inc.; North Carolina State University: Raleigh, NC, 1998.

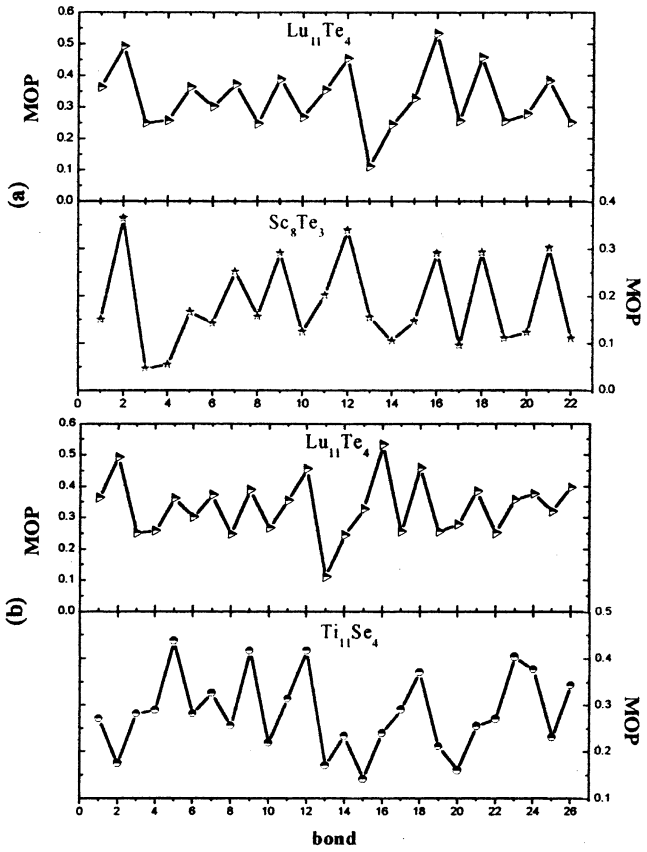

Figure 5. Comparison of EHTB R−R bond populations (ordered in ascending atom numbers, see the Supporting Information) for (a) $Lu_{11}Te_4$ versus Sc_8Te_3 and (b) $Lu_{11}Te_4$ versus $Ti_{11}Se_4$. Bonding function is the most important variable, even for interchanged atom pairs, in Figures 1−3.

seen for bond 2, the diagonal M2−M2 separation, appears to reflect chain distortions and a MOP decrease in the sheets in $Ti_{11}Se_4$. Logically, bond 15 for M9−M11 is appreciably diminished when Se2 and Se3 become neighbors, and the opposite is true for bond 23, M15−M16, as Ti16 is now more interior. Finally, differences in the placement of the transposed metal dimers mean that the Ti10−Ti15 interaction (bond 16) is relatively longer and weaker than Lu10−Lu11.

In general, the apparent charge and bond population trends in the pairs of structural comparisons $Lu_{11}Te_4$−Se_8Te_3 and $Lu_{11}Te_4$−$Ti_{11}Se_4$ shown in Figures 4 and 5 present both clearer and less qualitative measures of what one tends to "see" or imagine in looking at just structural (geometric) pictures and distances. Moreover, an additional point has been made frequently; bond distances may not parallel bond strength (overlap populations) measures well,[5,11] particularly when matrix effects or, presumably, delocalization become large in certain situations. Matrix effects are especially hard to judge in compact and complex structures as considered here. Relative Coulombic terms still remain difficult to assess well in intercomparing complex structures.

Acknowledgment. This research was supported in part by the National Science Foundation, Solid State Chemistry, via Grant DMR-0129785, and was carried out in the facilities of the Ames Laboratory, DOE. Some of the research was also supported by a Hundred Talents Program Award of the Chinese Academy of Sciences to L. C. in 2003.

Supporting Information Available: Tables of crystallographic and refinement data, anisotropic displacement parameters, extended Hückel parameters, and the bond-ordering system for Figure 5. This material is available free of charge via the Internet at http://pubs.acs.org.

IC0401142